


RESEARCH ARTICLE

Open Access



# Prediction of soil erosion and sediment transport in a mountainous basin of Taiwan

Yuei-An Liou<sup>1,2\*</sup> , Quang-Viet Nguyen<sup>1,3</sup>, Duc-Vinh Hoang<sup>1,4</sup> and Duy-Phien Tran<sup>1,5</sup>

## Abstract

Soil erosion substantially implicates global nutrient and carbon cycling of the land surface. Its monitoring is crucial for assessing and managing global land productivity and socio-economy. The Zhuoshui River Basin, the largest catchment, in Taiwan is highly susceptible to soil erosion by water due to extremely high rainfall, rugged terrain, easily eroded soil, and intensively agricultural cultivation over the steep land. Hence, this study examines the annual soil erosion rate for 2005, 2011, and 2019 and the average long-term soil erosion and sediment yield (SY) during 2005–2019. Coupling of the Revised Universal Soil Loss Equation (RUSLE) and sediment delivery ratio (SDR) models is implemented using remote sensing and GIS techniques. The soil erosion rate is classified into five classes, namely *mild* (0–10 t ha<sup>-1</sup> year<sup>-1</sup>), *moderate* (10–50 t ha<sup>-1</sup> year<sup>-1</sup>), *moderately severe* (50–100 t ha<sup>-1</sup> year<sup>-1</sup>), *severe* (100–150 t ha<sup>-1</sup> year<sup>-1</sup>), and *very severe* (> 150 t ha<sup>-1</sup> year<sup>-1</sup>). Over one half of the total area is categorized as *moderate* and *moderately severe* classes, and one-third of the whole basin as *severe* and *very severe* classes. Recently, *mild* and *moderate* classes increase, while *moderately severe*, *severe*, and *very severe* decrease. During 2005–2019, the annual soil loss rate ranges from 0.00 to 6,881.88 t ha<sup>-1</sup> year<sup>-1</sup> with an average rate of 122.94 t ha<sup>-1</sup> year<sup>-1</sup>. Among the SDR models, the RUSLE combined with the SDR model with the length and slope gradient of mainstream shows satisfactory sediment yield estimation. Predictably, the downstream receives a massive sediment delivery from all upper streams (246.06 × 10<sup>6</sup> t year<sup>-1</sup>), and the percent bias values for all sub-basins are below ± 39.0%. The study provides a rapid approach to investigate soil erosion and sediment yield, and it can be applied to the other basins in Taiwan. More importantly, information about spatial patterns of soil erosion and SY is critical to establish suitable measures to achieve effective watershed planning and optimize the regional productivity and socio-economy. The proposed approach is potentially to identify risk areas, conduct scenario estimation for management, and perform spatiotemporal comparison of soil erosion, while adjustment in the empirical formulas of the proposed approach may be needed when it is applied to the other regions, especially outside Taiwan.

**Keywords:** RUSLE, Sediment yield, Soil erosion, Sediment delivery ratio, Zhuoshui River Basin

## 1 Introduction

Erosion is a process that makes the soil particles displaced by agents, such as water, wind, and gravity (Lal 1994; Zhang et al. 2019; Xie et al. 2021a). It can be triggered by natural disturbance, especially associated with heavy rainfall over the cyclone-prone regions, e.g., East

of Southeast Asian countries (Liu et al. 2015; Liou et al. 2016, 2018; Nguyen et al. 2021; Pandey et al. 2021). In addition, the human-included perturbation can accelerate the soil erosion rate (SER), resulting in adverse impacts on soil productivity, waterway obstruction, water quality decline, etc. (Lal 1994). To calculate soil loss, field measurement is considered as the most reliable asset, but it is challenging to clarify the main cause of the erosion process (Morgan 2005). Besides, it is rather time-consuming and costly to conduct field measurements. Therefore, it is impractical to count on this traditional

\*Correspondence: yueian@csrsr.ncu.edu.tw

<sup>1</sup> Center for Space and Remote Sensing Research, National Central University, No. 300, Jhongda Rd., Jhongli District, Taoyuan City 320317, Taiwan, ROC  
Full list of author information is available at the end of the article

approach to estimate the soil loss rate to establish the management plans for soil loss mitigation at regional scale. To overcome the limitations, soil erosion modeling is useful means to obtain essential information on spatial patterns and trends of erosion severity to help the land-use stakeholders build scenarios for further analysis in consideration of the current or potential land uses (Karydas et al. 2012; Millington 1986; Xie et al. 2021b). Currently, soil erosion models can be divided into empirically-, conceptually-, and physically-based models to simulate spatiotemporal erosion at different scales (Merritt et al. 2003). Understanding the spatial distribution of erosion rate within a watershed is necessary for planning soil and water conservation (Vigiak and Sterk 2001). Although physically-based models can express the natural mechanisms in erosion and deposition processes by integrating into a complex model, these models require massive input data, making them inefficient for soil and water conservation planning (Ketema and Dwarakish 2019; Vigiak and Sterk 2001).

Until now, the Revised Universal Soil Loss Equation (RUSLE), recognized as an empirical soil erosion model, is the most widely used worldwide (Pandey et al. 2021). Because of its flexibility and less input requirement, it is found with some limitations in predicting gully, stream bank erosion, sediment deposition, and sediment yield (SY) (Alewell et al. 2019; Batista et al. 2017; Ketema and Dwarakish 2019; Lin et al. 2002). To estimate the sediment yield, the combination of soil erosion and sediment delivery ratio (SDR) is commonly used (Swarnkar et al. 2018; Walling 1983). Under such circumstance, the coupled RUSLE-SDR model has been employed to predict SY in the previous studies (Almagro et al. 2019; Ghani et al. 2013; Jain and Kothiyari 2000; Lin et al. 2002; Rajbanshi and Bhattacharya 2020; Swarnkar et al. 2018; Walling 1983). The SDR depends on geomorphological characteristics of a watershed, such as drainage size, relief, stream length, slope gradient of mainstream (Ferro and Minacapilli 1995; Walling 1983). Its value tends to increase with decreasing catchment area. Like the RUSLE, an SDR equation is developed in a particular region so that it is limited when it is applied for the regions outside its original area (Alewell et al. 2019; Ferro and Minacapilli 1995). Despite its drawbacks, the RUSLE, together with Geographic Information System (GIS) is popularly used in modeling soil erosion by water globally, particularly at a large scale (Batista et al. 2017). The RUSLE model uses six parameters that affect the soil erosion process by water, including climate, land use/land cover, soil property, topographic condition, and conservation practice. Currently, the RUSLE model is standard for soil loss prediction mentioned in the Soil and Water Technical Regulations by Taiwan's Council of Agriculture (Chou 2009).

Antecedent studies in Taiwan attempted to develop empirical equations as the RUSLE input parameters and SDR of various basins that have been further incorporated into the Soil and Water Conservation Bureau's Handbook for designing the soil and water conservation facilities in controlling the sediment volume (Lin et al. 2015). However, it requires detailed land-use information that is challenging to acquire under rugged terrains. Also, it is difficult to simulate slope length and steepness of topography with complex condition at a large scale if the suggested methods are utilized. The SDR formulas in Taiwan were developed in the past, while they are subjective to the biophysical conditions, particularly human factors (Soil and Water Conservation Bureau [SWCB] 2019). Until now, the coupled RUSLE-SDR has been rarely seen in Taiwan. Hence, its predictive capacity is now also questionable, especially in environmental conditions of rugged topography with extremely high rainfall. According to Kao and Milliman (2008), the annual average sediment yield from the 16 Taiwanese rivers is sixty times higher than the global average ( $150 \text{ t km}^{-1} \text{ year}^{-1}$ ). Thus, the integrated RUSLE and SDR model, which enables a rapid and reliable assessment of soil erosion and SY at a basin scale, is still needed for the effective basin management in Taiwan.

The Zhuoshui River Basin (ZRB), located in the central region, is the largest catchment in Taiwan. It produces the highest amount of sediment loads compared to the other river basins (such as Tamshui, Zengwen, Gaoping, and Hualien) in Taiwan (Chiang et al. 2019). A vast amount of sediment delivery mainly results from the geological characteristics with geographical distribution prone to heavy precipitation, typhoons, and landslides (Chiang et al. 2019).

Hence, this study aims to (1) apply the RUSLE model to predict the soil loss rate for 2005, 2011, and 2019 and the corresponding average SERs; (2) combine the RUSLE and SDR models to estimate the long-term sediment yield for each sub-basin; and (3) examine how well the coupled RUSLE-SDR model perform SY prediction as compared with the observed sediment at gauge stations under the complex biophysical conditions of the ZRB. The modeled outcomes of SER and SY would be helpful for the local authority in proposing further practical measures for soil and water conservation.

## 2 Methods/experiment

### 2.1 Study area

The Zhuoshui River, also called Choshui River, is the longest river in Taiwan. It originates from the west part of the central mountain range and travels through four counties (Nantou, Changhua, Yunlin, and Chiayi) before joining the Taiwan Strait. The main stream of the ZRB

is ~187 km in length with basin area of ~3200 km<sup>2</sup> (Kuo et al. 2017). The upper basin is characterized by a fragile slate, shale, and sandstone vulnerable to erosion forcing (Kuo et al. 2017). This basin mainly lies between 0 and 3873 m above sea level, and a significant portion is characterized by steep and rugged terrains (Fig. 1). Annually, this basin receives an average rainfall of 2500 mm, significantly varying from 1500 to 4000 mm over the lowland plains and mountainous areas. The rainy season from May to October accumulates more than 75% of its total annual precipitation (Kuo et al. 2017).

## 2.2 Data used

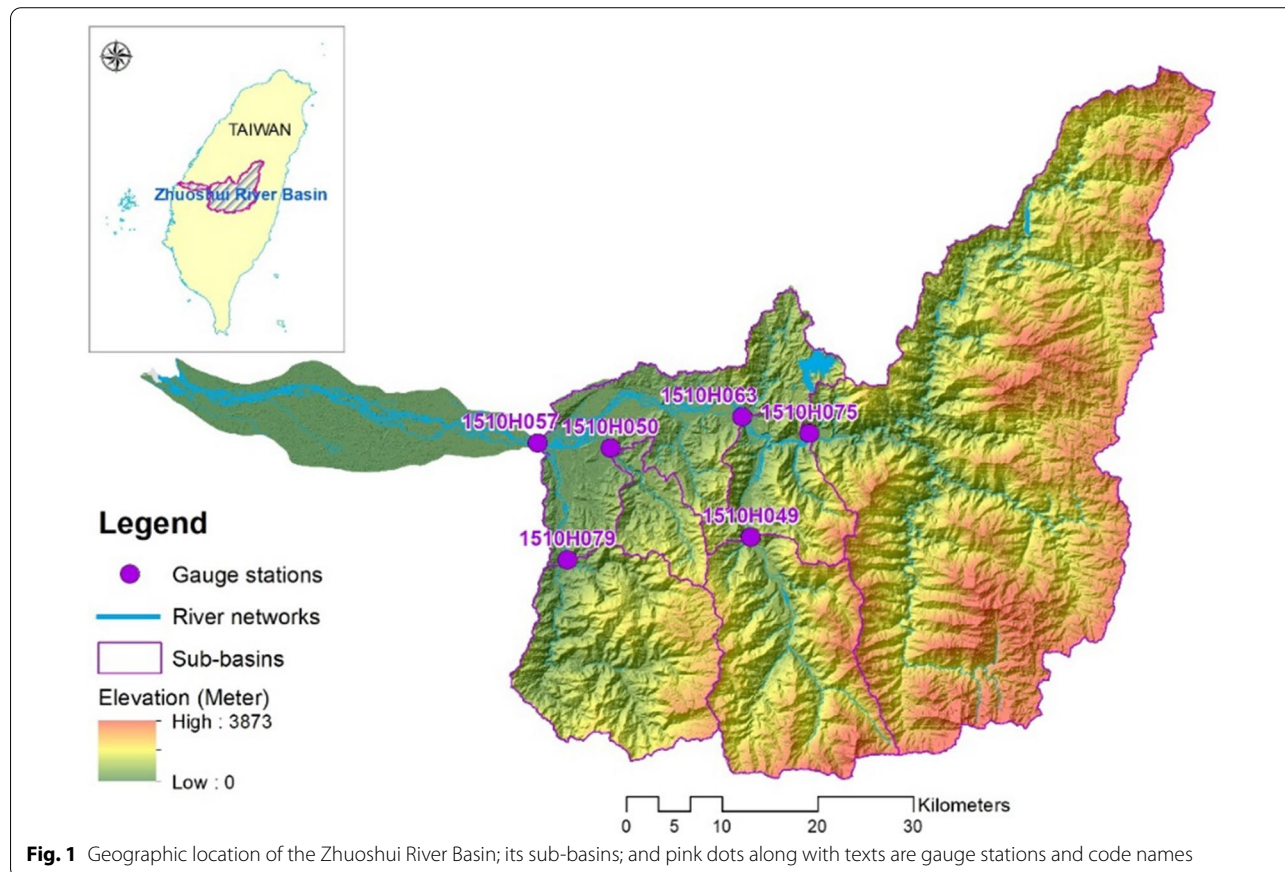
To achieve the objects of the study, we used various satellite, GIS, and station level data. The details of primary data are given below.

- (1) Digital elevation model (DEM) from Shuttle Radar Topographic Mission (SRTM), known as SRTM DEM at 30-m resolution, was collected from United States Geological Survey website (downloaded at <https://earthexplorer.usgs.gov/>);
- (2) Four scenes of Landsat 8 OLI TIRS data (Scene 1: Path=118, Row=43; Scene 2: Path=118,

Row=44; Scene 3: Path=117, Row=43; Scene 4: Path=117, Row=44) were downloaded from the United States Geological Survey website with 20, 19, and 20 images for 2005, 2010, and 2019, respectively;

- (3) Long-term average annual precipitation at 49 meteorological stations located in and around the ZRB were collected from the Central Weather Bureau, Taiwan;
- (4) Soil map was obtained from the Taiwan Agricultural Research Institute, Council of Agriculture; and
- (5) Sediment and water discharge at 6 gauge stations from 2005 to 2018 were collected from the Water Resources Agency, Taiwan.

To diminish the effects of high cloud frequency, we prioritized Landsat 8 OLI TIRS series of images during the dry season (January to April). The land-use/land-cover (LULC) classification was defined by four scenes of Landsat 8 OLI TIRS data. Also, Landsat images were processed on the Google Earth Engine Platform to compute the Normalized Different Vegetation Index (NDVI)-based C factor used in the RUSLE model.



### 2.3 Implementation process

Figure 2 presents a comprehensive step-by-step procedure of the study.

Firstly, the RUSLE inputs were identified to simulate SER for the three years of interest. Landsat data were prepared to retrieve the NDVI and LULC for calculating the C and P factors, while the other factors were estimated from rainfall, soil, and DEM data. Secondly, we stacked all the input layers at a 30-m resolution to model the SER for 2005, 2011, and 2019, and the corresponding long-term average SERs. Thirdly, the DEM analysis was conducted to determine sub-basin boundary and its size, mainstream length, and mainstream bed slope, which served as input parameters of the SDR formulas. The SDR values were calculated for each sub-basin with respect to the three SDR formulas of concern. Fourthly, the long-term SY was estimated by the RUSLE and SDR models. Finally, the coupled RUSLE-SDR performance respective to each SDR model was evaluated by comparison with the observed sediment discharge.

### 2.4 LULC retrieval from Landsat image

Before LULC classification, some preprocessing steps were conducted to enhance the image quality. First, geometric, atmospheric, and topographic corrections were implemented on each Landsat image. Next, cloud removal was implemented to detect the cloud-shadow pixels, which were then replaced by cloudless pixels from the other images to create a single cloud-free

Landsat image for the three different years. Random Forest was selected as a classifier to produce the LULC maps because of its superiority over the other machine learning algorithms (Talukdar et al. 2020). It has advantages in coping with noise of the unbalanced and discrete or continuous datasets (Breiman 2001) to achieve high accuracy (Abdullah et al. 2019; Pal et al. 2021). In order to collect training samples for LULC classification, we scrutinized high-resolution images from Google Earth, different band composites, and indices (NDVI, Normalized Different Bare Land Index, Urban Index). To obtain a better result of the LULC classification, some types were divided into smaller classes for better matching the spectral profile to create a preliminary map. Thereafter, the final LULC map was regrouped into five different classes, namely forest, built-up land, bare land, agricultural land, and water body.

### 2.5 Determination of the RUSLE inputs

The RUSLE was originally developed by Wischmeier and Smith (1965) and then modified by Renard et al. (1997). It can be described as:

$$A = R \times K \times L \times S \times C \times P \tag{1}$$

where  $A$  is the average soil loss rate ( $t\ ha^{-1}\ year^{-1}$ ),  $R$  is the rainfall erosivity ( $MJ\ mm\ ha^{-1}\ h^{-1}\ year^{-1}$ ),  $K$  is the soil erodibility ( $t\ h\ MJ^{-1}\ mm^{-1}$ ),  $L$  is the slope length (dimensionless),  $S$  is the slope steepness,  $C$  is the cover

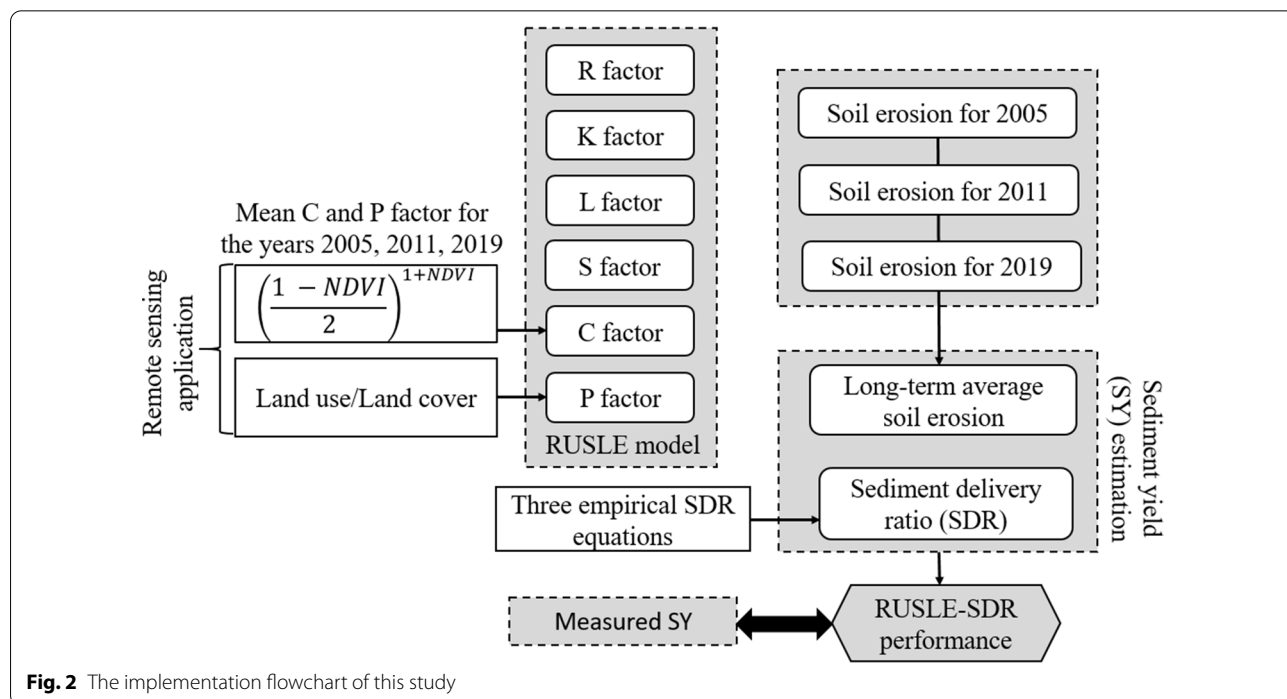


Fig. 2 The implementation flowchart of this study

and management (dimensionless), and  $P$  is the conservation practice (dimensionless).

**2.5.1 Rainfall Erosivity (R factor)**

The R factor indicates the energy of precipitation that can detach and transport soil particles from the surface to the other sites. It depends on the amount and magnitude of rainfall. The R formula was developed for a given region (Panditharathne et al. 2019; Renard et al. 1997; Wischmeier and Smith 1978). We selected the R equation mentioned by SWCB (2019) for the Nantou County nearby the ZRB:

$$R = 17.02 \times 0.020653 \times P^{1.35072} \tag{2}$$

where  $R$  is the rainfall erosivity ( $\text{MJ mm ha}^{-1} \text{h}^{-1} \text{year}^{-1}$ ), and  $P$  is the annual average rainfall (mm).

Because a high variation in topographic conditions might affect the precipitation spatial pattern, the long-term average annual rainfall data at 49 meteorological stations and their geographical locations were used to simulate spatial pattern of the annual average rainfall using the co-kriging interpolation.

**2.5.2 Soil erodibility (K factor)**

The K factor expresses the ability of soil to resist the force of rainfall and surface runoff. Wischmeier and Smith (1978) and Renard et al. (1997) used the K equation for the RUSLE, which requires the soil texture, structure, organic matter content, soil permeability, and infiltration. However, these parameters might not be available or match the other soil classifications. Thus, alternative methods were developed to estimate the K factor with less soil information than the original formula. For example, Williams et al. (1983) used sand, silt, clay, and organic content, whereas David (1988) based on one more parameter, pH value, and El-Swaify and Dangler (1976) only used the textural information and base saturation.

In this study, the K factor was extracted from the soil index (KI) of Taiwanese soil types via KI value’s relation to the  $K$  value of the USLE model (Table 1). The  $K$  value was determined by the following equation (SWCB 2019):

$$K = (KI - 1)/200 \tag{3}$$

where  $K$  is the soil erodibility ( $\text{t h MJ}^{-1} \text{mm}^{-1}$ ), and KI is the Taiwanese soil index.

**2.5.3 Slope length (L) and steepness (S) factors**

The LS factor consists of slope length (L) and steepness (S), strongly affecting soil erosion. In this study, the slope length was calculated by following the method proposed by Desmet and Govers (1996), in which the authors used the concept of the contributing area. It can be retrieved

**Table 1** K value obtained from KI value based on Taiwanese soil types (adapted from (SWCB 2019))

Soil types	KI value	K
Diluvial Material Yellow Soils	10	0.045
Diluvium Red Soils	7	0.030
Metamorphic Rock Pale Colluvial Soils	8	0.035
Miscellaneous Lands	11	0.050
Precipitous Areas	8	0.035
Sandstone-Shale Darkish Colluvial Soils	7	0.030
Sandstone-Shale Lithosols	6	0.025
Sandstone-Shale Order Alluvial Soils	12	0.055
Sandstone-Shale Pale Colluvial Soils	14	0.065
Sandstone-Shale Yellow Soils	7	0.030
Sandstone-Shale-Slate Calcareous Alluvial Soils	10	0.045
Sandstone-Shale-Slate Non-Calcareous Alluvial Soils	13	0.060
Slate Calcareous Alluvial Soils	3	0.010
Slate Calcareous Older Alluvial Soils	11	0.050
Slate Non-Calcareous Alluvial Soils	11	0.050

from flow algorithms by using DEM (Desmet and Govers 1996; Huang et al. 2007). The S factor was computed according to Zevenbergen and Thorne (1987). This LS factor algorithm is appropriate for modeling soil erosion at landscape-scale and can represent complex topography (Desmet and Govers 1997; Panagos et al. 2015). To simulate the LS factor, the SRTM DEM at 30-m resolution was put into the SAGA (System for Automated Geoscientific Analyses) software via its terrain analysis tool.

**2.5.4 Cover and management (C factor)**

The C factor represents the ability of vegetation to protect the soil surface from raindrop and runoff. RS data with high spatiotemporal coverage have been intensively used to extract the C value instead of the LULC-based method. The C factor is estimated using NDVI transformation proposed by various studies, such as Durigon et al. (2014) and van der Knijff et al. (1999). The equation from the verification of several watersheds in Taiwan (Chou 2009) was used in this study:

$$C = \left[ \frac{1 - \text{NDVI}}{2} \right]^{1 + \text{NDVI}} \tag{4}$$

The Google Earth Engine was used to acquire Landsat time-series data for the years 2005, 2011 and 2019. Initially, preprocessing was required for further analysis. Firstly, the CFMask algorithm was used for the removal of clouds and cloud shadows (Foga et al. 2017). Secondly, the topographic illumination correction was conducted to minimize the effect of rugged topographic conditions to achieve consistency of spatiotemporal measurements (Hurni et al. 2019) whereby applying a physical method

proposed by Dymond and Shepherd (1999). Finally, the yearly mean Landsat data were obtained for the years of concern and exported as a single cloud-free image. All previous processes are referred the tool for preprocessing Landsat image as described by Hurni et al. (2017). After that, NDVI-based transformation in Eq. (4) was utilized to calculate the mean C value of the three different years.

### 2.5.5 Conservation practice (P factor)

The P factor represents the effects of controlled measurements to reduce the rate of the amount of runoff and raindrop that strike on the soil surface. The common support practices are contour farming, terracing, strip cropping, and grassed waterways (Ghosal and Das Bhat-tacharya, 2020). The lower the P value, the more effective the support practice promotes the deposition of soil particles (Alewell et al. 2019).

Within the RUSLE, a list of P values corresponding to a wide range of support practice conditions are mainly derived from the experiment data at plots or field scale. Therefore, while transferring the P factor from a field scale to a large scale based on GIS-based modeling, it is considered as the least reliable of the RUSLE factors because of the lack of spatial information (Alewell et al. 2019). The P estimation is primarily controlled by two determinants, e.g., land-use types and the terrain slope (Nyssen et al. 2009; Tian et al. 2021). The topographic conditions are characterized by steep and rugged features, so that they might strongly affect soil erosion process. Hence, the equation developed by Wenner (1981) that shows the linear relationship between the slope and amount of conservation practice (P) (Ghosal and Bhat-tacharya 2020; Lufafa et al. 2003) was selected:

$$P = 0.2 + 0.03 \times S \quad (5)$$

where P is the amount of conservation practice, and S is the slope in percentage.

### 2.6 Sediment delivery ratio and sediment yield estimation

The SDR is defined as the proportion of gross erosion expected to travel to the outlet of a given catchment area (Ferro and Minacapilli 1995). It is influenced by various environmental variables, such as rainfall, vegetation, topography, and soil properties and their complicated interactions (Walling 1983). Due to the complex mechanism of basin sediment transport, the physical-based distributed models are still rarely seen (Wu et al. 2017). Thus, the empirical SDR developed for a given watershed is widely used for estimating SDR (Lim et al. 2005). The empirical SDR equations have been discussed and can be used for Taiwan (SWCB 2019). Out of 10 equations, this study considered three empirical equations as they provide satisfactory results. Other equations cannot

give satisfactory results as they lack some basic information and are proposed for the other specific catchments of reservoirs. Hence, they cannot be used in the current analysis. The selected SDR equations were developed for 10 on-stream reservoirs; and the watersheds of Zengwen Reservoir and eight others (Chen and Lai 1999; SWCB 2019). These equations were described in Eqs. (6, 7, and 8), respectively.

$$SDR_1 = 249 \times A^{-0.316} \quad (6)$$

$$SDR_2 = 165.67 \times A^{-0.24} \quad (7)$$

$$SDR_3 = 129.02 \times (L/\sqrt{Sr})^{-0.19} \quad (8)$$

where A is the watershed area in km<sup>2</sup>, L is the length of mainstream in km, and Sr is the slope gradient of stream bed in percentage (%).

After determining the gross erosion from the RUSLE model and SDR, sediment yield for a given catchment can be defined as (Jain and Kothiyari 2000):

$$SY_i = SDR_i \times A_i \quad (9)$$

where SY<sub>i</sub> is the sediment yield for a grid cell i, SDR<sub>i</sub> is the soil delivery ratio for a cell i, and A<sub>i</sub> is soil loss rate predicted by the RUSLE model (t ha<sup>-1</sup> year<sup>-1</sup>) for a grid cell i.

### 2.7 Computation of observed sediment

The measured sediment data from the Water Resource Agency of Taiwan over the period of 2005–2018 were computed for 6 gauge stations. At each gauge station, the water and suspended sediment discharge were sampled two to three times a month. The rating curve method, which presents an exponential regression between the measured daily flow discharge Q (m<sup>3</sup> s<sup>-1</sup>) and measured daily sediment discharge Q<sub>s</sub> (t day<sup>-1</sup>), was utilized to estimate the annual amount of suspended sediment discharge. This method is widely used for gauge stations where sampling frequency is unusual or insufficient (Ahn and Steinschneider 2018; Hung et al. 2018). To reduce the residuals between the calculated and observed suspended sediment discharge, a modified rating curve method proposed by Kao et al. (2005) was applied.

## 3 Results

### 3.1 Final LULC maps

The final LULC maps extracted from Landsat images were validated for the five classes: water, forest, bare land, built-up land, and agricultural land. The random forest in mapping LULC showed a satisfactory performance. More specifically, the LULC maps for 2005, 2011, and 2019 obtained high overall accuracy values (0.91, 0.93, and

0.90, respectively) and Kappa values (0.91, 0.92, and 0.90, respectively).

The spatial distribution of LULC types and their statistical information for 2005, 2011, and 2019 are shown in Fig. 3 and Table 2, respectively. Forest occupied the largest portion of the total area (over 75%), while built-up land shared smallest percentage of the whole area (around 1.10%). Agricultural land was ranked at the second dominant LULC type (11.0%), followed by bare land (5.80%). In general, the ZRB has undergone a minor change among LULC types over the 15-year period. Forest and bare land slightly reduced in 2011 and then

increased by under 0.50% in 2019. In contrast, agricultural land recently decreased by 2.05% after a small increase of 0.43% from 2005 to 2011. Water and built-up lands gradually increased.

### 3.2 The RUSLE modeling

#### 3.2.1 Estimating the RUSLE factors

Rainfall erosivity in the ZRB ranged from 4575.03 to 17,544.86 MJ mm ha<sup>-1</sup> h<sup>-1</sup> year<sup>-1</sup> with a mean value of 12,351.11 MJ mm ha<sup>-1</sup> h<sup>-1</sup> year<sup>-1</sup> and standard deviation of 2394.30 MJ mm ha<sup>-1</sup> h<sup>-1</sup> year<sup>-1</sup>. The value of this parameter tended to increase from low plains to

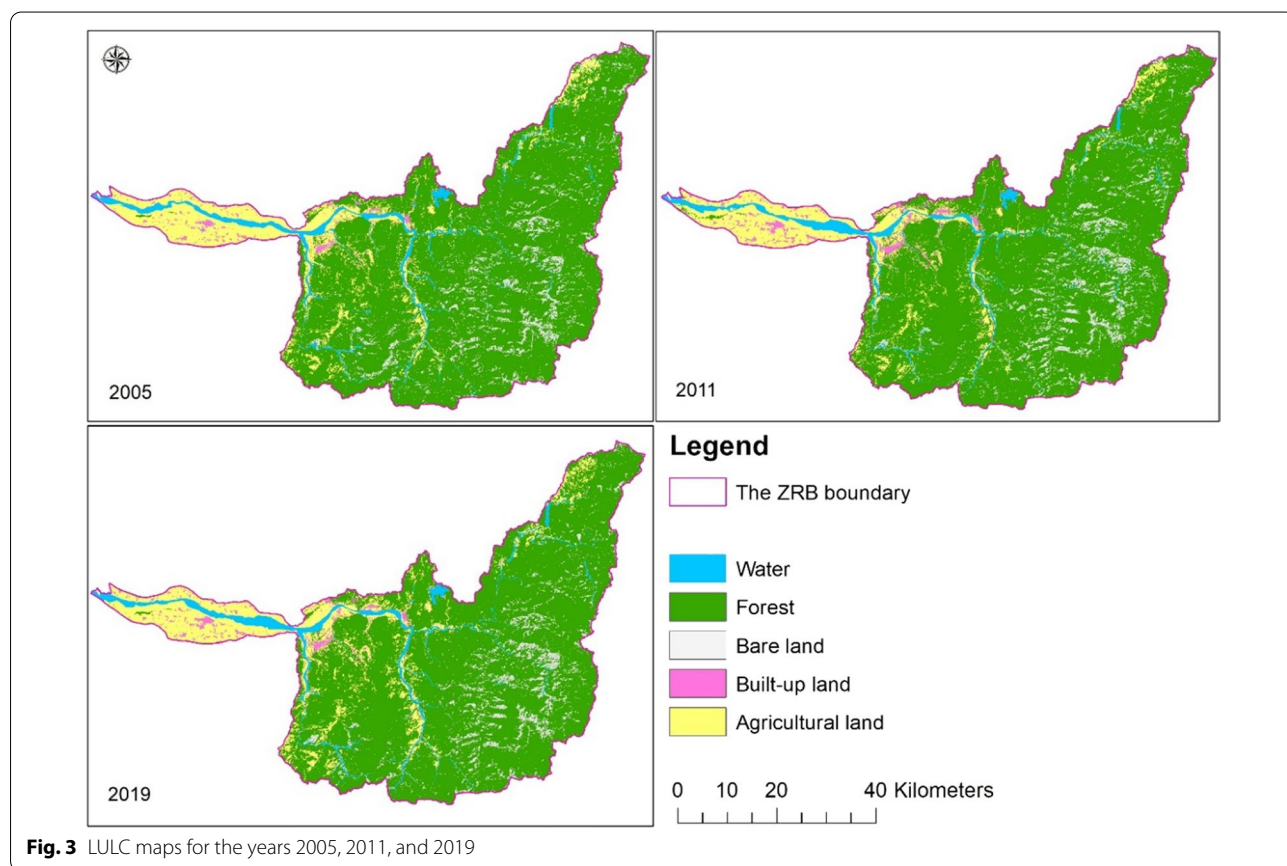


Fig. 3 LULC maps for the years 2005, 2011, and 2019

Table 2 Descriptive information on LULC types

LULC types	2005		2011		2019	
	Area (ha)	percentage (%)	Area (ha)	percentage (%)	Area (ha)	percentage (%)
Water	12,733.65	4.02	13,593.69	4.30	12,455.28	4.78
Forest	239,234.04	75.61	237,657.96	75.11	240,571.98	75.75
Bare land	20,558.34	6.50	18,491.49	5.84	21,053.25	6.47
Built-up land	3604.41	1.14	5054.94	1.60	6175.17	1.90
Agricultural land	40,284.90	12.73	41,626.26	13.16	36,168.66	11.11

mountainous regions (Fig. 4a). The  $K$  value varied from 0.01 to 0.065 t h MJ<sup>-1</sup> mm<sup>-1</sup>, and the mean  $K$  value was 0.04 t h MJ<sup>-1</sup> mm<sup>-1</sup>, as presented in Fig. 4b.

The spatial distribution of the combined LS factor is presented in Fig. 4c. Due to the rugged topography, the LS factor obtained a mean value of 8.15. The highest value was found on the slope land nearby the water body, while the bottom of the valley or low plain received the lowest value close to zero. The increase in the LS value means that the runoff and soil erosion are likely to speed up at a higher rate.

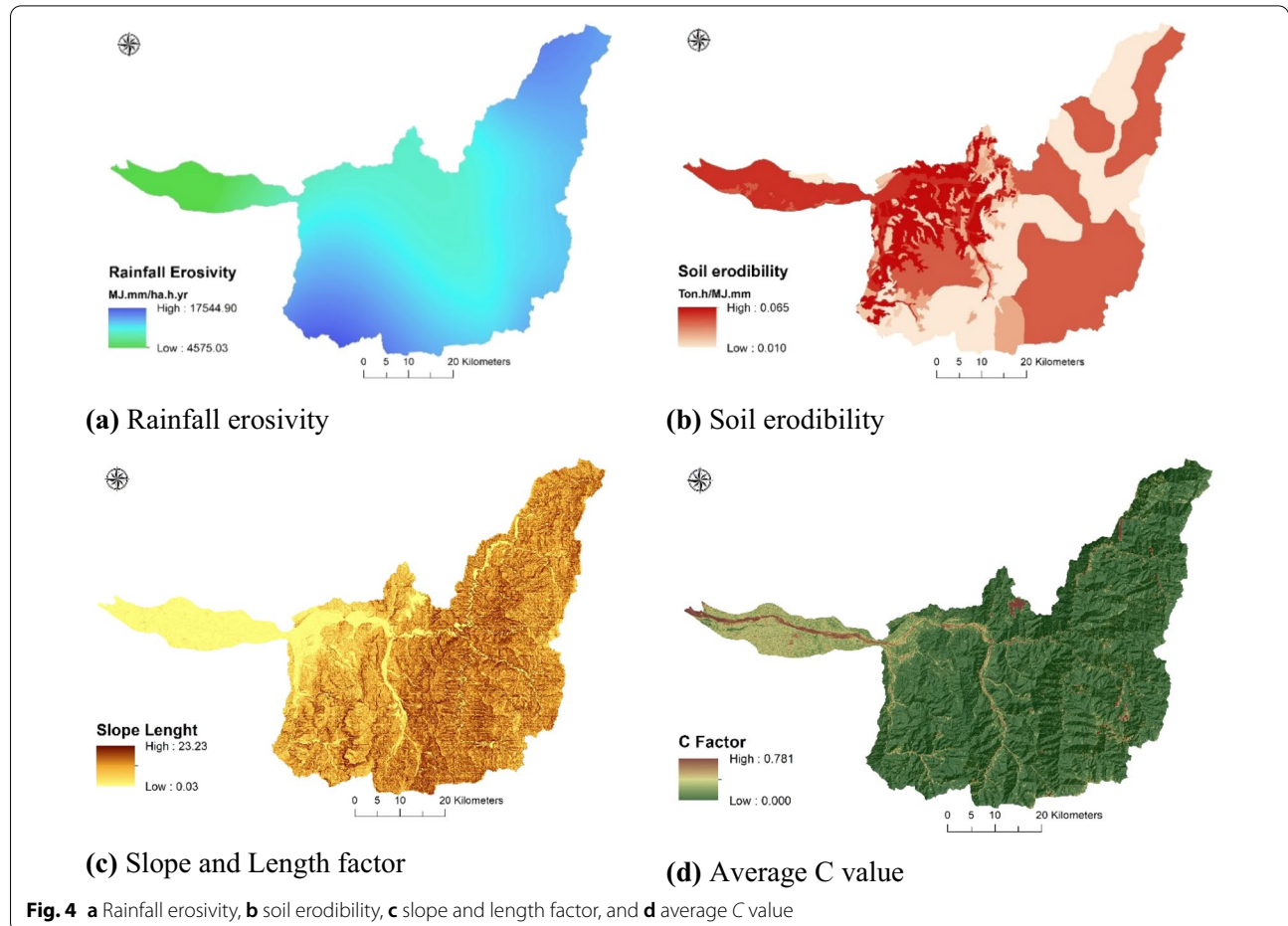
As shown in Fig. 4d, the  $C$  value ranged from 0 to 0.781 with a mean value of 0.06. The lower  $C$  value represents a more effective ability of vegetation cover to protect the soil surface from erosion forcing. Generally, forests at the high elevation obtained the lowest  $C$  value, close to 0, while agricultural crops distributed in the river valley or low plain had a higher  $C$  value. In contrast, bare land obtained the highest  $C$  value.

The  $P$  value for agricultural land was derived from Eq. (5). It was set to be 0 for the water body and built-up land, and 1 for the forest and bare land. The LULC types

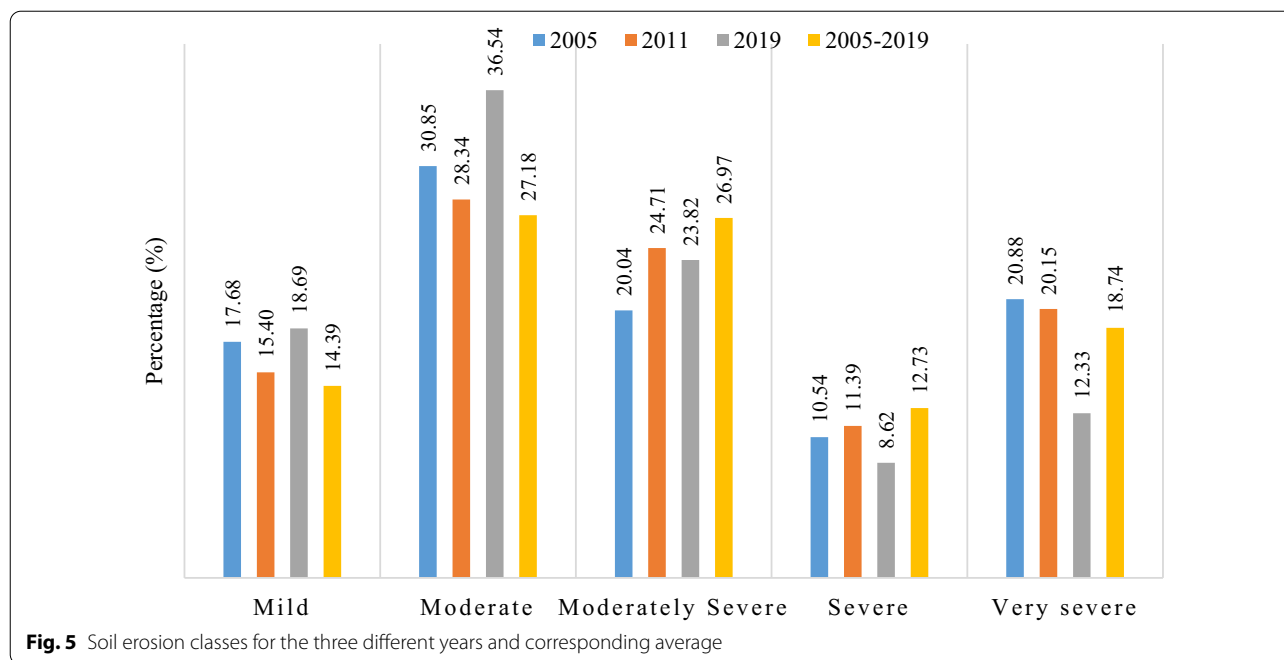
associated with slope gradient were gathered to compute the  $P$  value for the years of interest. Results reveal that the  $P$  value slightly fluctuated because agricultural land remained stable during the study period.

### 3.2.2 Soil erosion dynamics

The soil erosion rate was estimated by overlaying the five thematic layers designed in raster format with 30-m resolution. The long-term average soil erosion rate was calculated by averaging soil erosion rate. Then, the soil erosion rate was classified into 5 soil erosion severity classes (Kimaro et al. 2008; Turkelboom 1999), namely mild (0–10 t ha<sup>-1</sup> year<sup>-1</sup>), moderate (10–50 t ha<sup>-1</sup> year<sup>-1</sup>), moderately severe (50–100 t ha<sup>-1</sup> year<sup>-1</sup>), severe (100–150 t ha<sup>-1</sup> year<sup>-1</sup>), and very severe (> 150 t ha<sup>-1</sup> year<sup>-1</sup>). The soil erosion class and its percentage area are presented in Fig. 5. The moderate class was dominated and followed by moderately severe class, while severe class occupied a smallest proportion of the ZRB over the given years. The mild and moderate class experienced a slight drop by around 2% before increasing by 3% and 8% from 2011 to 2019, respectively. Conversely, the moderately







severe and severe class rose by 4.31% and 0.85% from 2005 to 2011, respectively, and then reduced by 0.89% and 2.77% from 2011 to 2019, respectively. A decreasing trend was observed at the very severe class over the study period, particularly a remarkable reduction by 7.82% from 2011 to 2019.

Figure 6 shows spatial distribution of soil erosion classes during 2005–2019. It is observed that the moderate and moderately severe classes occupied a large portion with 54.15% of the total area. The mild class accounted for around 14.39% and the remaining severe and very severe classes together shared 31.47%. The SER ranged from 0.00 to 6,881.88 t ha<sup>-1</sup> year<sup>-1</sup>, and the average rate was 122.94 t ha<sup>-1</sup> year<sup>-1</sup>.

In general, the mild class occurred in the low plain, bottom of river valleys, and high mountains with closed vegetation. The moderate class is distributed dispersedly in different kinds of terrains. Conversely, the severe and very severe erosion rates (over 100 t ha<sup>-1</sup> year<sup>-1</sup>) happened on the sloping land with a sparse cover like bare land or upland agricultural crops.

### 3.2.3 Soil erosion intensity at different LULC types

Table 3 illustrates a significant difference in SER among LULC types. Bare land suffered the most detrimental impacts of soil erosion at the highest rate of over 390 t ha<sup>-1</sup> year<sup>-1</sup>, while water and built-up land were not affected by the soil erosion process. Although forest lessened the risk of soil erosion, the average SER was still high at over 100 t ha<sup>-1</sup> year<sup>-1</sup>. Additionally, agricultural

land was eroded at a rate above 22 t ha<sup>-1</sup> year<sup>-1</sup>. In brief, soil erosion recently occurred on main LULC types that reduce intensity as compared to the previous years.

### 3.3 Sediment yield prediction

To calculate the three empirical SDR equations, two major steps were carried out. Firstly, the spatial boundary of each sub-basin respective to its gauge station was delineated by using the DEM analysis via the Hydrology and Surface tool of ArcGIS software (as presented in Fig. 1); then, the size of sub-basins and their slope gradient and mainstream were identified. Each sub-basin represents its whole upstream area with water flowing into its outlet (gauge station).

As shown in Table 4, the SDR<sub>1</sub> and SDR<sub>2</sub> at each sub-basin ranged from 20.02% to 61.13%. The SDR<sub>2</sub> was slightly higher than SDR<sub>1</sub>, except for sub-basin 1510H050. As for the SDR<sub>3</sub>, its value varied from 57.26 to 89.33%. The SDR<sub>3</sub> for a certain sub-basin gave higher SDR values than the two equations SDR<sub>1</sub> and SDR<sub>2</sub> within the ZRB.

As for each sub-basin, the gross erosion value was computed from the RUSLE. Then, it was combined with the three SDRs to determine sediment yield according to Eq. (9).

Table 5 shows a large variation of the SY values following the SDR equations among sub-basins. The SY estimation produced by the SDR<sub>1</sub> and SDR<sub>2</sub> gave a slight difference (around 10 × 10<sup>6</sup> t year<sup>-1</sup>) compared to the SDR<sub>3</sub> (approximately two times higher) for each sub-basin.

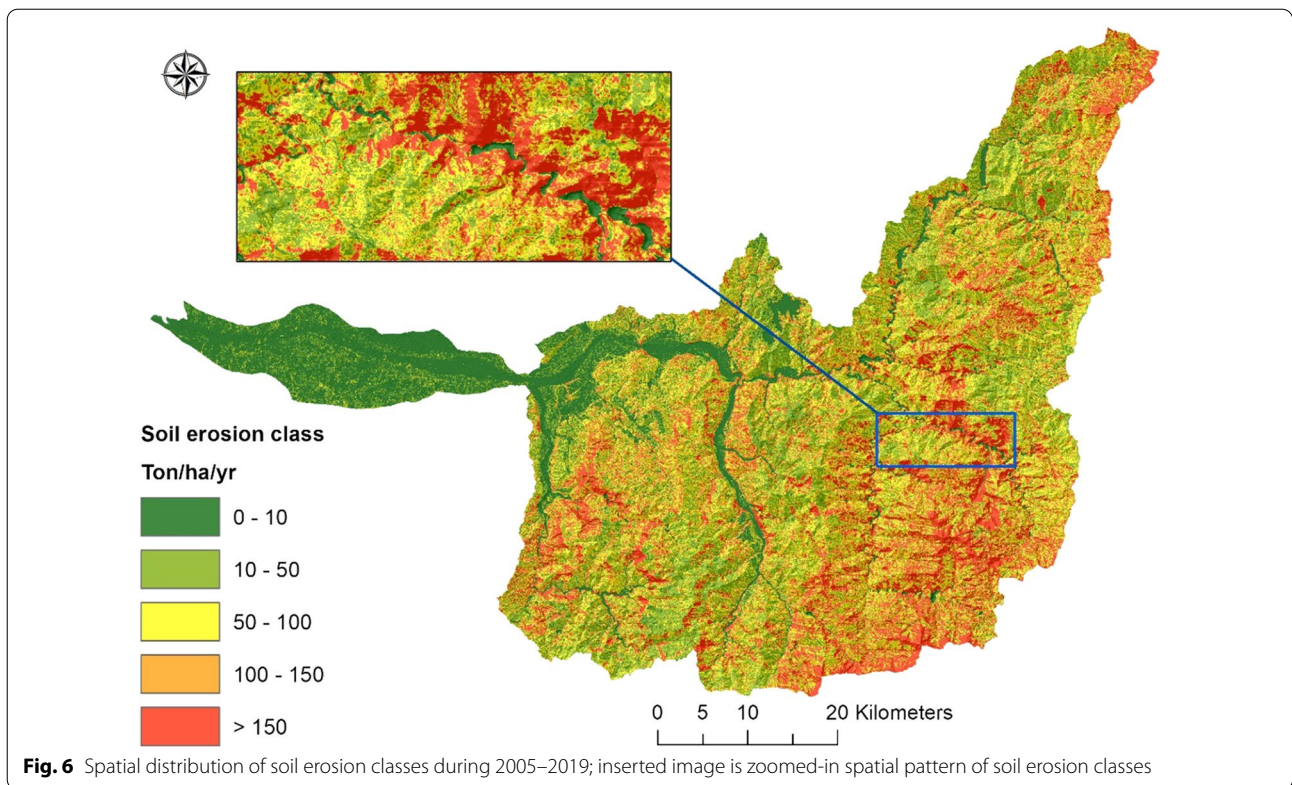


**Table 3** Average soil erosion rate corresponding to LULC types

LULC types	2005		2011		2019	
	Average value and its standard variation ( $t\ ha^{-1}\ year^{-1}$ )					
Forest	124.59	217.47	119.81	208.70	102.84	316.11
Bare land	521.92	737.61	537.10	732.10	396.58	684.64
Agricultural land	32.41	96.09	31.16	84.11	22.79	72.05

Soil erosion rate of water and built-up land is zero

**Table 4** Sediment delivery ratio for each sub-basin

Sub-basin	Gauge station	Area ( $km^2$ )	SDR <sub>1</sub>	SDR <sub>2</sub>	SDR <sub>3</sub>
1510H050	Yanping	85.15	61.13	57.02	89.33
1510H079	Longmen	360.37	38.75	40.33	78.62
1510H049	Neimaopu	367.17	38.52	40.15	81.42
1510H075	Bǎoshí	1576.42	24.31	28.30	63.09
1510H063	Yufeng	2096.46	22.21	26.43	61.37
1510H057	Zhang Yun	2911.13	20.02	24.43	57.26

Each sub-basin represents the whole upper areas where water flows into its gauge station; SDR<sub>1,2,3</sub> values were obtained from the three SDR equations, respectively

**Table 5** The predicted sediment yield ( $10^6\ t\ year^{-1}$ ) with respect to the three SDR equations

Sub-basin	Gross erosion (A)	SY <sub>1</sub>	SY <sub>2</sub>	SY <sub>3</sub>
1510H050	8.30	5.07	4.73	7.41
1510H079	46.15	17.88	18.61	36.28
1510H049	52.77	20.33	21.19	42.97
1510H075	284.05	69.05	80.39	179.22
1510H063	352.93	78.40	93.28	216.59
1510H057	429.71	86.05	104.97	246.06

Gross erosion (A) is obtained from the annual average soil erosion rate for 2005, 2011, and 2019 by using the RUSLE model; SY<sub>1,2,3</sub> values are obtained from the RUSLE and SDR<sub>1,2,3</sub> equations, respectively

**Table 6** Annual suspended sediment discharge ( $10^6$  t year<sup>-1</sup>) at gauge stations

Sub-basin	Gauge station	Period	Number of measured days	Observed sediment
1510H050	Yanping	4/2005–2018	328	12.00
1510H079	Longmen	10/2009–2018	267	45.99
1510H049	Neimaopu	2005–2018	398	32.22
1510H075	Bǎoshí	2005–2018	443	156.50
1510H063	Yufeng	2005–2018	401	278.46
1510H057	Zhang Yun	2005–2018	407	325.78

### 3.4 Validation of sediment yield estimation

In this study, annual suspended sediment discharge at 6 gauge stations was calculated by using the modified rating curve derived from the daily water discharge from 2005 to 2018 (measured days over 250). The results of the observed sediment calculation are presented in Table 6.

Table 6 illustrates that gauge stations experienced a large variation in suspended sediment discharge. At a dependent sub-basin, 1510H075 (Bǎoshí) located at the farthest distance from the downstream obtained a value of suspended sediment discharge at  $156.50 \times 10^6$  (t year<sup>-1</sup>). In contrast, 1510H050 (Yanping) nearby the downstream received the lowest value at  $12.00 \times 10^6$  (t year<sup>-1</sup>). The difference between these two stations was around 13 times. In this period, the annual suspended sediment discharge at downstream gauge (Zhang Yun) standing for the whole upstream area was about  $325.78 \times 10^6$  (t year<sup>-1</sup>). That is, the Zhuoshui River annually produced a massive amount of sediment from its upper streams.

To evaluate the model performance in SY prediction, Pearson’s correlation coefficient ( $r$ ), coefficient of determination ( $R^2$ ), and percent bias (PBIAS) were calculated from the long-term simulated SY and measured SY for each sub-basin.

$$PBIAS(\%) = \frac{\sum_{i=1}^n O_i - P_i}{\sum_{i=1}^n O_i} \times 100 \quad (10)$$

where  $O_i$  is the observed value,  $P_i$  is the predicted value, and  $n$  is the number of measurements.

As shown in Table 7, the SY estimation obtained from the equation  $SDR_{1,2,3}$  reveals a strong relationship with the observed SY, in which both  $r$  and  $R^2$  values were over 0.90. However, the PBIAS derived from the  $SDR_3$  was smaller than the  $SDR_{1,2}$ . Meanwhile, the length and slope gradient of mainstream at each sub-basin gave a better sediment yield prediction in combination with the RUSLE than the catchment size. The  $SDR_1$  and  $SDR_2$  caused estimation errors, which were over two times

**Table 7** Model performance evaluation corresponding to three empirical SDR equations

Model performance	SDR <sub>1</sub>	SDR <sub>2</sub>	SDR <sub>3</sub>
Pearson’s correlation coefficient ( $r$ )	0.96	0.97	0.97
Coefficient of determination ( $R^2$ )	0.92	0.93	0.95
PBIAS (%)			
1510H050	57.74	60.59	38.26
1510H079	61.11	59.53	21.11
1510H049	36.91	34.25	-33.35
1510H075	55.88	48.63	-14.52
1510H063	71.85	66.50	22.22
1510H057	73.59	67.78	24.47

higher than the  $SDR_3$  at each sub-basin, except for sub-basin 151H049. The  $SDR_1$  and  $SDR_2$  underestimated the sediment yield at all sub-basins, while the  $SDR_3$  resulted in the same situation, except for sub-basins 1510H049 and 1510H075 (overestimation). The estimation errors from the  $SDR_3$  at each sub-basin ranged from 14.52 to 38.26%. Compared to the previous studies (Donigian 2002; Moriasi et al. 2007), the RUSLE and  $SDR_3$  achieved satisfactory performance at the ZRB.

### 4 Discussion

In this study, the RUSLE coupled with the empirical SDR equation performs satisfactorily in estimating SY at the ZRB. It reveals that the model’s capacity in modeling is unexpectedly limited when it is applied for local physical conditions. Due to uncertainty in identifying the RUSLE parameters and SDR, the model performance should be carefully considered and adapted to local rainfall patterns, vegetation cover, and soil characteristics (Alewell et al. 2019). This study used the empirical equations for determining the RUSLE inputs and SDRs (except for the P and LS factors), which were developed in the environmental conditions of Taiwan. Also, the selected methods for determining the C, P, and LS factors are derived from remote sensing data and LS algorithm to compensate the rugged terrains in Taiwan. In contrast, the suggested methods by SWCB (2019) reveal disadvantages as applied for a large scale. For example, the C and P factors based on a lookup table require detailed land-use information and its corresponding management practice, while the LS factor is developed by experiment based on a one-direction regular slope and a standard plot. Hence, the used methodologies may reduce uncertainty in soil erosion and SY prediction. Also, this work provides a rapid approach for soil erosion assessment, which is adequate for a mountainous basin.

This study highlighted that among the three SDR candidates, the SDR<sub>3</sub> illustrated a better prediction of sediment transport than the SDR<sub>1</sub> and SDR<sub>2</sub> at each sub-basin when combined with the RUSLE. Obviously, the controlling factors of the SDR are extremely complex related to watershed characteristics, landforms, hydrological and climatic conditions, and anthropogenic management (Wu et al. 2017). The SDR<sub>3</sub> is identified by two determinants: the length of mainstream and slope gradient of stream bed, which might explain sediment transport capability to the study basin. A long mainstream has great chances to receive eroded materials from hillslopes. Also, with a high gradient, mainstream is more capable of transporting eroded materials to down streams (USDA-SCS 1972). The SDR<sub>3</sub> matches with some previous SDRs, which are proposed for a watershed with short length and steep slope (Bartholic 2004). While the SDR<sub>1</sub> and SDR<sub>2</sub> based on the size of basin area insufficiently identify the SDR value in this study, the SDR value tends to decrease with the catchment area and depends on many factors (Smith and Wilcock 2015; Wu et al. 2017). A larger basin has more probabilities to trap eroded materials and, then, lessen the amount of eroded materials traveling further to down streams (Bartholic 2004). This might be well explained for large and flat catchments. However, for catchments with short and high elevation variations, the sediment transport process may be efficiently presented by the slope and length of mainstreams.

The RUSLE-SDR<sub>3</sub> model fairly implemented at six sub-basins with the PBIAS values under  $\pm 39\%$  compared to previous studies (Donigian 2002; Moriasi et al. 2007). Meanwhile, the SDR<sub>3</sub> can estimate SDR for a large difference in sub-basin characteristics concerning the length of mainstream and slope gradient of stream bed. Thus, the coupled RUSLE-SDR<sub>3</sub> model can be potentially applicable for the other basins in Taiwan. Noticeably, the SDR value is determined by a wide range of decisive factors and complex processes (erosion, transportation, and deposition). Hence, further consideration is still needed to identify the SDR and achieve a better result of sediment prediction.

Several authors noted that a model should be validated without any calibration steps (Alewell et al. 2019; Sverdrup et al. 1995). This study directly utilized all inputs to simulate the SY, which was checked and validated with the observed SY. Currently, on-site plots for soil loss rate measurement are unavailable or difficult to obtain to validate the RUSLE performance at large scale (Cerdan et al. 2010), while the output of the RUSLE-SDR can be validated with the observed SY available at many gauge stations within the watershed. Although the physical-based models exhibit many advances in soil erosion modeling, empirical models often achieve more successfully and

are possible to perform (Morgan 2005). Managers, policy makers, planners demand the simple predictive tools to support decision-making processes rather than the complicated systems (Morgan 2005; Vigiak and Sterk 2001).

The RUSLE was designed to predict the annual average soil loss rate by inter-rill and rill erosion as it ignores gullies and stream bank erosion. Additionally, the existing SY models cannot fully account for gully, bank erosion, and mass movements (de Vente et al. 2013). These soil erosion processes occur simultaneously at a catchment scale, so that it is challenging to quantify typical sediment sources separately. Until now, modeling approaches in researching soil erosion and sedimentation process still need much more effort due to their limitations for various aspects (Dutta 2016). Currently, torrents, gullies, and riverbank erosions in Taiwan are mostly controlled by man-made works (Lin et al. 2002). Hence, this study assumes that inter-rill and rill erosions are the main sources of sediment production within the study basin. Despite the existing limitations, the RUSLE-SDR model with the assistance of GIS and RS was fairly conducted for the long-term estimation of SE and SY in the ZRB. Among the SDR models, the SDR model related to stream characteristics was appropriate in combination with the RUSLE to estimate SY under the complex biophysical conditions of the ZRB. It is important to note that the RUSLE-SDR approach enables to simulate the soil erosion and SY for the environmental conditions of the ZRB, where has been adversely suffering from soil erosion on sloping lands and sediment deposition at down streams. The proposed approach is potentially applicable to other catchments in Taiwan.

## 5 Conclusions

This study applied the RUSLE-SDR model with the support of geospatial analysis and RS data to estimate the annual and long-term average soil erosion and SY in the ZRB. The soil erosion rate is classified into five classes, namely *mild* (0–10 t ha<sup>-1</sup> year<sup>-1</sup>), *moderate* (10–50 t ha<sup>-1</sup> year<sup>-1</sup>), *moderately severe* (50–100 t ha<sup>-1</sup> year<sup>-1</sup>), *severe* (100–150 t ha<sup>-1</sup> year<sup>-1</sup>), and *very severe* (>150 t ha<sup>-1</sup> year<sup>-1</sup>). Over one half of the total area is categorized as *moderate* and *moderately severe* classes, and one-third of the whole basin as *severe* and *very severe* classes. Recently, *mild* and *moderate* classes increased, while *moderate severe*, *severe*, and *very severe* decreased. During 2005–2019, the annual soil erosion rate varied from 0.00 to 6881.88 t ha<sup>-1</sup> year<sup>-1</sup>, and the average rate was 122.94 t ha<sup>-1</sup> year<sup>-1</sup>. The SDR for each sub-basin extracted from mainstream length and slope gradient of the mainstream bed together with the RUSLE illustrates a better prediction of SY than those derived from the catchment size. Predictably,

downstream receives a massive sediment delivery from all upper streams ( $246.06 \times 10^6 \text{ t year}^{-1}$ ), and the PBIAS values for all sub-basins are below  $\pm 39.0\%$ . Spatial distribution of soil erosion rate and SY is valuable information for soil and water conservation, which support the local government in considering controlling measures to achieve sustainable agricultural development. Note that this study referred to the previous studies with involvement of empirical equations developed for Taiwan and then manipulated all available data for modeling to achieve satisfactory outcomes. Under such circumstance, the used methodology is potentially applicable to the other catchments in Taiwan, but it has to be adjusted to fit the local environment for the regions outside Taiwan.

#### Abbreviations

DEM: Digital elevation model; GIS: Geographical information system; LULC: Land use/land cover; NDVI: Normalized Different Vegetation Index; RS: Remote sensing; RUSLE: Revised Universal Soil Loss Equation; SDR: Soil delivery ratio; SER: Soil erosion rate; SRTM: Shuttle Radar Topographic Mission; SY: Sediment yield; ZRB: Zhuoshui River Basin.

#### Acknowledgements

The authors appreciate the United States Geological Survey (USGS) for providing the satellite data used in this study. We thank reviewers for providing constructive comments to improve our manuscript.

#### Author contributions

Conceptualization was done by QVN and YAL. Data curation was done by QVN, DPT, and DVH. Formal analysis was done by QVN. Funding acquisition was done by YAL. Investigation was done by QVN and DPT. Methodology was done by QVN. Project administration was done by YAL. Supervision was done by QVN and YAL. Writing of the original draft and reviewing, editing, revising, and finalization of the manuscript were done by YAL and QVN. All authors read and approved the final manuscript.

#### Funding

This work was supported by both Taiwan's Soil and Water Conservation Bureau, Council of Agriculture and Taiwan's Ministry of Science and Technology (MOST) under the project's codes 109保發-11.1-保-01-06-001(3), and MOST 108-2111-M-008-036-MY2.

#### Availability of data and materials

Please contact author for data requests.

#### Declarations

#### Competing interests

The authors declare that they have no competing interest.

#### Author details

<sup>1</sup>Center for Space and Remote Sensing Research, National Central University, No. 300, Jhongda Rd., Jhongli District, Taoyuan City 320317, Taiwan, ROC. <sup>2</sup>National Museum of Marine Science and Technology (NMMST), No. 367, Beining Rd., Zhongzheng Dist., Keelung City 202010, Taiwan, ROC. <sup>3</sup>University of Sciences, Hue University, 77-Nguyen Hue, Hue 530000, Vietnam. <sup>4</sup>Vietnam Academy for Water Resources, 171-Tay Son, Hanoi 100000, Vietnam. <sup>5</sup>Institute of Geography, Vietnam Academy of Science and Technology, 18-Hoang Quoc Viet, Hanoi 100000, Vietnam.

Received: 24 April 2022 Accepted: 28 September 2022

Published online: 12 October 2022

#### References

- Abdullah AYM, Masrur A, Adnan MSG, Baky MAA, Hassan QK, Dewan A (2019) Spatio-temporal patterns of land use/land cover change in the heterogeneous coastal region of Bangladesh between 1990 and 2017. *Remote Sens* 11(7):7. <https://doi.org/10.3390/rs11070790>
- Ahn KH, Steinschneider S (2018) Time-varying suspended sediment-discharge rating curves to estimate climate impacts on fluvial sediment transport. *Hydrol Process* 32(1):102–117
- Alewell C, Borrelli P, Meusburger K, Panagos P (2019) Using the USLE: chances, challenges and limitations of soil erosion modelling. *Int Soil Water Conserv Res* 7(3):203–225. <https://doi.org/10.1016/j.iswcr.2019.05.004>
- Almagro A, Thome TC, Colman CB, Pereira RB, Junior JM, Rodrigues DBB, Oliveira PTS (2019) Improving cover and management factor (C-factor) estimation using remote sensing approaches for tropical regions. *Int Soil Water Conserv Res* 7(4):325–334
- Bartholic J (2004) Predicting sediment delivery ratio in saginaw bay watershed. Institute of Water Research, Michigan State University, East Lansing
- Batista PVG, Silva MLN, Silva BPC, Curi N, Bueno IT, Acérbí Júnior FW, Davies J, Quinton J (2017) Modelling spatially distributed soil losses and sediment yield in the upper Grande River Basin—Brazil. *CATENA* 157:139–150. <https://doi.org/10.1016/j.catena.2017.05.025>
- Breiman L (2001) Random forests. *Mach Learn* 45(1):5–32
- Cerdan O, Govers G, Le Bissonnais Y, Van Oost K, Poesen J, Saby N, Gobin A, Vacca A, Quinton J, Auerswald K (2010) Rates and spatial variations of soil erosion in Europe: a study based on erosion plot data. *Geomorphology* 122(1–2):167–177
- Chen SC, Lai YC (1999) Estimating the sediment delivery ratio in rivers and watersheds. *J Chin Soil Water Conserv* 30(1):47–57
- Chiang LC, Wang YC, Liao CJ (2019) Spatiotemporal variation of sediment export from multiple Taiwan watersheds. *Int J Environ Res Public Health* 16(9):7. <https://doi.org/10.3390/ijerph16091610>
- Chou WC (2009) Modelling watershed scale soil loss prediction and sediment yield estimation. *Water Resour Manag* 24(10):2075–2090. <https://doi.org/10.1007/s11269-009-9539-6>
- David WP (1988) Soil and water conservation planning: policy issues and recommendations. <https://core.ac.uk/download/pdf/6506014.pdf>. Accessed 8 Sept 2022
- de Vente J, Poesen J, Verstraeten G, Govers G, Vanmaercke M, Van Rompaey A, Arabkhedri M, Boix-Fayos C (2013) Predicting soil erosion and sediment yield at regional scales: where do we stand? *Earth Sci Rev* 127:16–29. <https://doi.org/10.1016/j.earscirev.2013.08.014>
- Desmet P, Govers G (1996) A GIS procedure for automatically calculating the USLE LS factor on topographically complex landscape units. *J Soil Water Conserv* 51(5):427–433
- Desmet P, Govers G (1997) Comment on 'Modelling topographic potential for erosion and deposition using GIS'. *Int J Geogr Inf Sci* 11(6):603–610
- Donigian AS (2002) Watershed model calibration and validation: the Hspf experience. *Proc Water Environ Fed* 2002(8):44–73. <https://doi.org/10.2175/193864702785071796>
- Durigon V, Carvalho D, Antunes M, Oliveira P, Fernandes M (2014) NDVI time series for monitoring RUSLE cover management factor in a tropical watershed. *Int J Remote Sens* 35(2):441–453
- Dutta S (2016) Soil erosion, sediment yield and sedimentation of reservoir: a review. *Model Earth Syst Environ*. <https://doi.org/10.1007/s40808-016-0182-y>
- Dymond JR, Shepherd JD (1999) Correction of the topographic effect in remote sensing. *IEEE Trans Geosci Remote Sens* 37(5):2618–2619
- El-Swaify SA, Dangler EW (1976) Erodibilities of selected tropical soils in relation to structural and hydrologic parameters
- Ferro V, Minacapilli M (1995) Sediment delivery processes at basin scale. *Hydrol Sci J* 40(6):703–717
- Foga S, Scaramuzza PL, Guo S, Zhu Z, Dilley RD Jr, Beckmann T, Schmidt GL, Dwyer JL, Hughes MJ, Laue B (2017) Cloud detection algorithm comparison and validation for operational Landsat data products. *Remote Sens Environ* 194:379–390
- Ghani A, Lihan T, Rahim S, Musthapha M, Idris W, Rahman Z (2013) Prediction of sedimentation using integration of RS, RUSLE model and GIS in Cameron Highlands, Pahang, Malaysia. Paper presented at the AIP conference proceedings

- Ghosal K, Das Bhattacharya S (2020) A review of RUSLE model. *J Indian Soc Remote Sens* 48(4):689–707. <https://doi.org/10.1007/s12524-019-01097-0>
- Huang JC, Kao SJ, Hsu ML, Liu YA (2007) Influence of Specific Contributing Area algorithms on slope failure prediction in landslide modeling
- Hung C, Lin GW, Kuo HL, Zhang JM, Chen CW, Chen H (2018) Impact of an extreme typhoon event on subsequent sediment discharges and rainfall-driven landslides in affected mountainous regions of Taiwan. *Geofluids*
- Hurni K, Van Den Hoek J, Fox J (2019) Assessing the spatial, spectral, and temporal consistency of topographically corrected Landsat time series composites across the mountainous forests of Nepal. *Remote Sens Environ* 231:11225
- Hurni K, Heinimann A, Würsch L (2017) Google earth engine image pre-processing tool: background and methods
- Jain MK, Kothiyari UC (2000) Estimation of soil erosion and sediment yield using GIS. *Hydro Sci J* 45(5):771–786. <https://doi.org/10.1080/02626660009492376>
- Kao S, Milliman JD (2008) Water and sediment discharge from small mountainous rivers, Taiwan: the roles of lithology, episodic events, and human activities. *J Geol* 116(5):431–448
- Kao SJ, Chan SC, Kuo CH, Liu KK (2005) Transport-dominated sediment loading in Taiwanese rivers: a case study from the Ma-an Stream. *J Geol* 113(2):217–225
- Karydas CG, Panagos P, Gitas IZ (2012) A classification of water erosion models according to their geospatial characteristics. *Int J Digit Earth* 7(3):229–250. <https://doi.org/10.1080/17538947.2012.671380>
- Ketema A, Dwarakish GS (2019) Water erosion assessment methods: a review. *ISH J Hydraul Eng*. <https://doi.org/10.1080/09715010.2019.1567398>
- Kimaro DN, Poesen J, Msanya BM, Deckers JA (2008) Magnitude of soil erosion on the northern slope of the Uluguru Mountains, Tanzania: interrill and rill erosion. *CATENA* 75(1):38–44. <https://doi.org/10.1016/j.catena.2008.04.007>
- Van der Knijff J, Jones R, Montanarella L (1999) Soil erosion risk assessment in Italy. Citeseer
- Kuo CW, Chen CF, Chen SC, Yang TC, Chen CW (2017) Channel planform dynamics monitoring and channel stability assessment in two sediment-rich rivers in Taiwan. *Water*. <https://doi.org/10.3390/w9020084>
- Lal R (1994) Global overview of soil erosion. *Soil Water Sci Key Underst Glob Environ* 41:39–51
- Lim KJ, Sagong M, Engel BA, Tang Z, Choi J, Kim KS (2005) GIS-based sediment assessment tool. *CATENA* 64(1):61–80. <https://doi.org/10.1016/j.catena.2005.06.013>
- Lin CY, Lin WT, Chou WC (2002) Soil erosion prediction and sediment yield estimation: the Taiwan experience. *Soil Tillage Res* 68(2):143–152
- Lin BS, Thomas K, Chen CK, Ho HC (2015) Evaluation of soil erosion risk for watershed management in Shenmu watershed, central Taiwan using USLE model parameters. *Paddy Water Environ* 14(1):19–43. <https://doi.org/10.1007/s10333-014-0476-5>
- Liou YA, Liu JC, Wu MX, Lee YJ, Cheng CH, Kuei CP, Hong RM (2016) Generalized empirical formulas of threshold distance to characterize cyclone–cyclone interactions. *IEEE Trans Geosci Remote Sens* 54(6):3502–3512
- Liou YA, Liu JC, Liu CP, Liu CC (2018) Season-dependent distributions and profiles of seven super-typhoons (2014) in the Northwestern Pacific Ocean from satellite cloud images. *IEEE Trans Geosci Remote Sens* 56(5):2949–2957
- Liu JC, Liou YA, Wu MX, Lee YJ, Cheng CH, Kuei CP, Hong RM (2015) Analysis of interactions among two tropical depressions and typhoons Tembin and Bolaven (2012) in Pacific Ocean by using satellite cloud images. *IEEE Trans Geosci Remote Sens* 53(3):1394–1402
- Lufafa A, Tenywa M, Isabirye M, Majaliwa M, Woomer P (2003) Prediction of soil erosion in a Lake Victoria basin catchment using a GIS-based Universal Soil Loss model. *Agric Syst* 76(3):883–894
- Merritt WS, Letcher RA, Jakeman AJ (2003) A review of erosion and sediment transport models. *Environ Model Softw* 18(8–9):761–799. [https://doi.org/10.1016/s1364-8152\(03\)00078-1](https://doi.org/10.1016/s1364-8152(03)00078-1)
- Millington A (1986) Reconnaissance scale soil erosion mapping using a simple geographic information system in the humid tropics. In: Land evaluation for land-use planning and conservation in sloping areas, pp 64–81
- Morgan R (2005) Soil erosion and conservation. Wiley, New York, p 16
- Moriassi DN, Arnold JG, Liew MWV, Bingner RL, Harmel RD, Veith TL (2007) Model evaluation guidelines for systematic quantification of accuracy in watershed simulations. *Trans ASABE* 50(3):885–900. <https://doi.org/10.13031/2013.23153>
- Nguyen KA, Liou YA, Vo TH, Cham DD, Nguyen HS (2021) Evaluation of urban greenspace vulnerability to typhoon in Taiwan. *Urban for Urban Green* 63:127191
- Nyssen J, Poesen J, Haile M, Moeyersons J, Deckers J, Hurni H (2009) Effects of land use and land cover on sheet and rill erosion rates in the Tigray highlands, Ethiopia. *Z Geomorphol* 53(2):171
- Pal S, Das P, Mandal I, Sarda R, Mahato S, Nguyen KA, Liou YA, Talukdar S, Debanshi S, Saha TK (2021) Effects of lockdown due to COVID-19 outbreak on air quality and anthropogenic heat in an industrial belt of India. *J Clean Prod* 297:126674
- Panagos P, Borrelli P, Meusburger K (2015) A new European slope length and steepness factor (LS-Factor) for modeling soil erosion by water. *Geosciences* 5(2):117–126. <https://doi.org/10.3390/geosciences5020117>
- Pandey LYA, Liu JC (2021) Season-dependent variability and influential environmental factors of super-typhoons in the Northwest Pacific basin during 2013–2017. *Weather Clim Extremes* 31:100307
- Pandey S, Kumar P, Zlatic M, Nautiyal R, Panwar VP (2021) Recent advances in assessment of soil erosion vulnerability in a watershed. *Int Soil Water Conserv Res* 9(3):305–318. <https://doi.org/10.1016/j.iswcr.2021.03.001>
- Panditharathne D, Abeysingha N, Nirmanee K, Mallawatantri A (2019) Application of revised universal soil loss equation (Rusle) model to assess soil erosion in “Kalu Ganga” river basin in Sri Lanka. *Appl Environ Soil Sci* 2019
- Rajbanshi J, Bhattacharya S (2020) Assessment of soil erosion, sediment yield and basin specific controlling factors using RUSLE-SDR and PLSR approach in Konar River basin, India. *J Hydrol* 587:124935
- Renard K, Foster G, Weesies G, McCool D, Yoder D (1997) Predicting soil erosion by water: a guide to conservation planning with the Revised Universal Soil Loss Equation (RUSLE). *Agric Handb* 703:25–28
- Renard KG (1997) Predicting soil erosion by water: a guide to conservation planning with the Revised Universal Soil Loss Equation (RUSLE). United States Government Printing
- Smith SMC, Wilcock PR (2015) Upland sediment supply and its relation to watershed sediment delivery in the contemporary mid-Atlantic Piedmont (U.S.A.). *Geomorphology* 232:33–46. <https://doi.org/10.1016/j.geomorph.2014.12.036>
- Soil and Water Conservation Bureau (2019) General & basic investigation and analysis. [https://www.swcb.gov.tw/Home/eng/Statistics/show\\_detail?id=4038556633c8485fb14ca42a90361194](https://www.swcb.gov.tw/Home/eng/Statistics/show_detail?id=4038556633c8485fb14ca42a90361194). Accessed 19 Apr 2022
- Sverdrup H, Warfvinge P, Blake L, Goulding K (1995) Modelling recent and historic soil data from the Rothamsted Experimental Station, UK using SAFE. *Agr Ecosyst Environ* 53(2):161–177
- Swarnkar S, Malini A, Tripathi S, Sinha R (2018) Assessment of uncertainties in soil erosion and sediment yield estimates at ungauged basins: an application to the Garra River basin, India. *Hydro Earth Syst Sci* 22(4):2471–2485
- Talukdar S, Singha P, Mahato S, Pal S, Liou YA, Rahman A (2020) Land-use land-cover classification by machine learning classifiers for satellite observations—a review. *Remote Sens* 12(7):1135. <https://doi.org/10.3390/rs12071135>
- Tian P, Zhu Z, Yue Q, He Y, Zhang Z, Hao F, Guo W, Chen L, Liu M (2021) Soil erosion assessment by RUSLE with improved P factor and its validation: Case study on mountainous and hilly areas of Hubei Province, China. *Int Soil Water Conserv Res* 9(3):433–444. <https://doi.org/10.1016/j.iswcr.2021.04.007>
- Turkelboom F (1999) On-farm diagnosis on steepland erosion in Northern Thailand: integrating spatial scales with household strategies. Katholieke Universiteit Leuven, Leuven
- USDA-SCS (1972) Sediment sources, yields, and delivery ratios. National engineering handbook. Section 3, Sedimentation. In: USDA Washington, DC
- Vigiak O, Sterk G (2001) Empirical water erosion modelling for soil and water conservation planning at catchment-scale. *WIT Trans Ecol Environ* 46:10
- Walling DE (1983) The sediment delivery problem. *J Hydrol* 65(1–3):209–237
- Wenner C (1981) Soil conservation in Kenya, 81, 81b. In: Nairobi. <https://edepot.wur.nl/480199>. Accessed 8 Sept 2022
- Williams J, Renard K, Dyke P (1983) EPIC: A new method for assessing erosion's effect on soil productivity. *J Soil Water Conserv* 38(5):381–383
- Wischmeier WH, Smith DD (1965) Predicting rainfall-erosion losses from cropland east of the Rocky Mountains

- Wischmeier WH, Smith DD (1978) Predicting rainfall erosion losses: a guide to conservation planning. Department of Agriculture, Science and Education Administration
- Wu L, Liu X, Xy Ma (2017) Research progress on the watershed sediment delivery ratio. *Int J Environ Stud* 75(4):565–579. <https://doi.org/10.1080/00207233.2017.1392771>
- Xie W, Li X, Jian W, Yang Y, Liu H, Robledo LF, Nie W (2021a) A novel hybrid method for landslide susceptibility mapping-based GeoDetector and machine learning cluster: a case of Xiaojin County, China. *ISPRS Int J Geo Inf* 10(2):93. <https://doi.org/10.3390/ijgi10020093>
- Xie W, Nie W, Saffari P, Robledo LF, Descote P, Jian W (2021b) Landslide hazard assessment based on Bayesian optimization–support vector machine in Nanping City, China. *Nat Hazards (dordrecht)* 109(1):931–948. <https://doi.org/10.1007/s11069-021-04862-y>
- Zevenbergen LW, Thorne CR (1987) Quantitative analysis of land surface topography. *Earth Surf Proc Land* 12(1):47–56
- Zhang K, Wang S, Bao H, Zhao X (2019) Characteristics and influencing factors of rainfall-induced landslide and debris flow hazards in Shaanxi Province, China. *Nat Hazard* 19(1):93–105. <https://doi.org/10.5194/nhess-19-93-2019>

### Publisher's Note

Springer Nature remains neutral with regard to jurisdictional claims in published maps and institutional affiliations.

Submit your manuscript to a SpringerOpen<sup>®</sup> journal and benefit from:

- ▶ Convenient online submission
- ▶ Rigorous peer review
- ▶ Open access: articles freely available online
- ▶ High visibility within the field
- ▶ Retaining the copyright to your article

---

Submit your next manuscript at ► [springeropen.com](https://www.springeropen.com)

---